Applied Catalysis B: Environmental 220 (2018) 264–271

Contents lists available at ScienceDirect

Applied Catalysis B: Environmental

journal homepage: www.elsevier.com/locate/apcatb

Research Paper

Photo-triggered catalytic reforming of methanol over gold-Promoted, copper-Zinc catalyst at low ignition temperature

Yi-Chun Liao, Hsiao-Yu Huang, Yuh-Jeen Huang*

Department of Biomedical Engineering & Environmental Sciences, National Tsing Hua University, Hsinchu, 30013, Taiwan

ARTICLE INFO

Keywords:
Ignition temperature
Photocatalytic
POM reaction
Mechanisms

ABSTRACT

Lowering the ignition temperature in partial oxidation of methanol (POM), an exothermic reaction, is important for further application in hydrogen fuel cell development. This study has clearly revealed that photo-triggered catalytic partial oxidation of methanol (photo-POM) over gold-promoted copper-zinc catalyst decreased ignition temperature in response to 2–10% increments of gold content. In particular, $A_{10}CZ$ (Au/Cu/ZnO catalyst with 10% Au, 30% Cu, 60% Zn) effectively reduced the ignition temperature (T_i) to room temperature and maintained 95% S_{H2} (hydrogen selectivity) methanol–oxygen mixtures (volume 2:1) under 200 W UV light with a wavelength of 377 nm. During the ignition period, methoxy groups ($–OCH_3$) were adsorbed onto the A_4CZ surface, and then transferred to the intermediate formate state. The photo-generated electrons from ZnO were easily trapped by electronic acceptors, such as copper and gold, which was confirmed by in-situ X-ray absorption near-edge structure (XANES) spectra during photo-POM reaction. Gold also promotes the absorption of near UV light and significantly enhances the charge separation by extracting electrons from photo-excited ZnO, which consequently improves the photocatalytic activity at lower ignition temperature.

1. Introduction

Hydrogen production by partial oxidation of methanol (POM), an exothermic reaction, has many advantages, such as higher reaction rates and no heat supply required if the reaction reaches steady-state [1–3]. In the POM reaction, a catalyst of copper supported with zinc oxide (CZ) provides high H_2 selectivity; however, the application is limited when the minimum temperature at which the substance ignition (ignition temperature, Ti) is high (ca. 180 °C) and the optimum reaction temperature (Tr) is at ca. 250 °C [4]. Therefore, lowering the ignition temperature is an important issue.

Recently, photocatalytic hydrogen generation from water or methanol using a semiconductor catalyst like ZnO or TiO_2 has become an attractive solution to resolve global energy challenges [5–12]. Zinc oxide has been widely used as a photocatalyst because of its higher initial activity rates, absorption efficacy of solar radiations [13,14], higher flatband potential [15], and sufficient conduction band potential for reduction of H^+ to H_2 [16–18]. But photocatalytic efficiency is low, because of a low energy utilization rate resulting from its direct band gap of 3.37 eV (at room temperature) caused by recombination of photogenerated electron-holes and photocorrosion of ZnO catalyst [18].

Photogenerated charge separation is another key issue affecting the efficiency of the photocatalytic process. Transition metals are widely used as effective co-catalysts for photocatalytic reaction [19–21]. Loading promotes the creation of active sites for hydrogen evolution, which results in inhibited charge recombination and enhanced photocatalytic activity [22,23]. In particular, Cu-deposited materials, applied as important *p*-type narrow bandgap semiconductors, have been shown to improve the photocatalytic efficiency of wide bandgap semiconductors [24,25] and considered to be potential photocatalysts for H_2 generation from aqueous methanol solution [7,21,26]. Wu et al. [21] have shown that the loading of ~1.2 wt% Cu enhancement activity exhibited an up to 10-fold enhancement in photocatalytic activity of TiO_2 for H_2 production from aqueous methanol solution. Gomathisankar et al. [27] indicated that photocatalytic hydrogen production using ZnO photocatalyst with Cu deposition was approximately 130 times better than that obtained with bare ZnO. The function of CuO is to help charge separation and to act as a reduction site. Highly stable reduced states were observed, which was due to an efficient charge transfer process [28]. Hence, in this study, copper is utilized to enhance the performance of ZnO-based catalyst in the photo-POM reaction.

Additionally, light sensitivity and catalyst absorption are other factors to consider. The loaded metal, in particular Au [29–32] enhances light absorption capability [33–35]. Sarina et al. [36] showed that the density of conduction electrons on the surface of gold nanoparticles (AuNP) was much higher than that at the surface of any

* Corresponding author.
E-mail address: yjhuang@mx.nthu.edu.tw (Y.-J. Huang).

http://dx.doi.org/10.1016/j.apcatb.2017.08.050
Received 8 February 2017; Received in revised form 18 July 2017; Accepted 14 August 2017
Available online 20 August 2017

semiconductor. Greaves et al. [37] indicated that gold is active in photocatalysis due to the higher density properties of conduction electrons, and has a better affinity with many reactants. Other previous research [38–40] has reported that a Schottky barrier, formed at the metal and semiconductor interface, could serve as an efficient electron trap, thus preventing photo-generated, electron-hole recombination. In addition, oxygen can trap electrons to become active O_2^- species when receiving electrons from AuNP surface, enhancing surface redox and photocatalytic reaction [41,42].

Thus, our hypothesis assumes that POM reaction can be enhanced via illumination. Gold nanoparticles were used in this work to improve photocatalytic activity of CuZnO catalyst and reduce the ignition temperature in the POM reaction from methanol–oxygen mixtures (gas volume 2:1) under 200 W UV light with a wavelength of 377 nm. Moreover, in-situ diffuse reflectance infrared Fourier transform spectroscopy(DRIFTS)and in-situ X-ray absorption near-edge structure (XANES) spectroscopy were applied to expose the photo-POM mechanism and to characterize the roles of gold, copper, and zinc-oxide species in detail.

2. Experimental section

2.1. Catalyst preparation

The gold-copper-zinc oxide catalysts (A_xCZ, x% Au loadings (x = 0 − 10), 30% Cu, (100-x-30)% Zn) were prepared by deposition precipitation (DP) following co-precipitation (CP) [43,44]. $Cu(NO_3)_2$. $3H_2O$ and $Zn(NO_3)_2$. $6H_2O$ solutions were dropped into deionized water at 70 °C under sonication at pH7. Na_2CO_3 was used to adjust the pH value. After aging to pH8, the CuZn precipitates were filtrated, washed, and dried at 105 °C overnight. An appropriate amount of $HAuCl_4$ · $3H_2O$ was dropped into 70 °C, 500 mL deionized water after adding pulverized CuZn precipitates. After aging 1 h, Au_xCuZn precipitates were filtrated, washed, and dried at 105 °C overnight. They were calcined in air at 400 °C for 2 h and then ground into size 60–80 mesh for catalytic testing.

The nomenclature and preparation conditions of catalysts are summarized in Table 1.

2.2. Characterization

The compositions of the catalysts were analyzed by ICP-MS, Perkin Elmer-SCIEX ELAN 5000. Prior to the ICP measurement, 20 mg of catalyst were completely dissolved in acid solution (1.5 mL HNO_3 and 0.5 mL HCl) in a Teflon-coated autoclave at 493 K for 4 h.

X-ray powder diffraction patterns were identified by Rigaku (Japan)-TTRAX Ⅲ with 18 KW rotating anode, Cu target Kα (λ = 0.15406 nm) radiation. Twenty scanning angles ranged from 20° to 50° at a rate of 4° s^{-1}.

The surface area of catalysts was obtained by Micromeritics ASAP-2020. Samples were pre-treated in situ under vacuum at 573 K. The N_2 adsorption/desorption isotherms were measured at 77 K. The surface area of catalysts was calculated according to the Brunauer–Emmett–Teller (BET) method [45].

X-ray photoelectron spectroscopy (XPS) spectra were recorded on a photoelectron instrument, Kratos Axis Ultra DLD (Kratos Analytical Ltd, UK), under ultra-high vacuum. In this study, the catalysts were measured by X-ray, Al Ka radiation = 1486.6 eV. All measured binding energies were referred to C1 s line of adventitious carbon 285 eV. For the energy range, survey spectra were recorded from 1100 eV to 0 eV in increments of 0.1 eV; for metal species, in increments of 0.01 eV. Deconvolution of XPS spectra was performed with OriginPro software, Gauss function.

Particle-size distribution and TEM image were analyzed by a high resolution TEM (JEOL-2100, LaB_6 electron gun source, 200 kV) with a point resolution of 0.23 nm.

Reducibility of freshly calcined catalysts was characterized by H_2 temperature-programmed reduction (TPR), which is a widely used for investigating the reducibility of catalysts. Temperature profiles of the rate of hydrogen consumption were measured by a thermal conductivity detector (TCD). In each TPR run, a sample of 55 mg in a U-shape tube reactor of 4 mm inner diameter was reduced by 10% H_2/N_2 at a flow rate of 30 mL/min upon raising the sample temperature from room temperature to 300 °C with a heating ramp of 7 °C/min. The software used for peak integration was provided by Scientific Information Service Corporation (SISC).

Copper dispersions were calculated from a three-step analysis consisting of: (1) H_2 TPR of the CuO, (2) N_2O oxidation of Cu to Cu_2O, and (3) secondary H_2 temperature-programmed-reduction (S-TPR) of the formed Cu_2O surface species. First, H_2 TPR was conducted to get in-situ reduction of the CuO phase to Cu(0). The oxidation of surface Cu(0) to Cu_2O was carried out by continuous pure N_2O flow (60 mL/min) at room temperature for 1 h. After this, S-TPR was carried out on the freshly oxidized Cu_2O surface to reduce Cu_2O to Cu. The surface Cu dispersion is calculated from the area of S-TPR multiplied by 2 and divided by the area of H_2 TPR [46].

UV–vis absorption spectra were recorded using a UV–vis spectrophotometer (Hitachi UV3300).

To study the changes in the states of copper and gold species during the photocatalytic POM reaction, in-situ X-ray absorption near-edge structure (XANES) spectrum analysis of catalysts was conducted at the 17C beam line of the National Synchrotron Radiation Research Center (NSRRC), Hsinchu, Taiwan. The electron storage ring was operated at 1.5 GeV with a stored current of 200 mA in a top-up injection mode. A Si (111) double crystal monochromator was used to select the energy. Absorption of Cu K-edge (8.979 KeV) and Au L_3-edge (11.919 KeV) was

Table 1
The nomenclature, preparation conditions and physicochemical properties of catalysts.

Catalyst	Nominal Au loading	Metal loading	Metal loading	Metal loading	Cu	Particle size (nm)[b]		BET surface area (m^2/g)	Distribution of elements, atom%[c]			
		Au (wt%)	Cu (wt%)	Zn (wt%)	dispersion (%)[a]	$d_{ZnO(101)}$	$d_{CuO(111)}$		Au_{4f}	Cu_{2p}	Zn_{2p}	Au^0/Au^{3+}
ZnO	–	–	–	–	–	10.08	–	–	–	–	–	–
CZ[d]	–	–	30.1	69.9	26.26	10.7	7.8	32.86	–	21.95	78.05	–
A_2CZ	2	1.8	30.4	67.8	28.53	9.33	6.5	41.36	11.86	21.80	66.34	0.1
A_3CZ	3	2.6	30.3	67.1	31.34	8.08	4.21	46.38	11.31	25.55	63.14	0.4
A_4CZ	4	3.8	30.4	65.8	33.66	6.51	4.14	49.34	13.05	28.39	58.56	1.21
$A_{10}CZ$	10	9.1	31.1	59.8	33.79	8.32	9.1	49.42	16.56	26.57	56.87	2.55

[a] Calculated Cu dispersion of catalysts by N_2O chemisorptions.
[b] Normal diameter estimated from XRD data using the Debye-Scherrer equation.
[c] Calculated from XPS.
[d] A_xCZ, x% Au loadings (x = 0–10), 30% Cu, (100-x-30)% Zn.

measured in transmission mode, respectively. The raw absorption data, with pre-edge and post-edge background subtracted, were normalized and fitted with Cu, Cu_2O, CuO, Au, $HAuCl_3$ standards.

Infrared spectra were collected using a Thermo Scientific Nicolet 6700 spectrometer equipped with a diffuse reflectance accessory and a MCT/A detector. Catalyst (0.1 g) was packed into the sample holder of the in-situ cell. The total flow gas through the in-situ cell was set at 70 mL/min. During the photocatalytic POM reaction, a 200 W xenon lamp (OB-200HX) with grating monochromator (wavelength of 377 nm) provided illumination on the in-situ cell. Thermostat-controller heating (HARRICK) was provided at 150 °C. The spectra were collected at a resolution of 4 cm^{-1} and an accumulation of 28 scans. Each spectrum was recorded every 30 s.

2.3. Photocatalytic reforming of methanol test

Catalytic activity measurements were conducted in a fixed-bed reactor (4 mm inner diameter) operating at atmospheric pressure. Freshly calcined catalysts were sieved through 60–80 mesh for testing. The liquid methanol was fed to the evaporator by piston pump, and the carrier gas Ar and reactant gas O_2 were introduced by a Brooks 5850E mass flow controller. The gas hourly space velocity (GHSV) and weight hourly space velocity (WHSV) were 60000 h^{-1} and 9.48 h^{-1}, respectively. The molar ratio of oxygen to methanol (O/M) was controlled at 0.5. The light was a 200 W xenon lamp (OB-200HX) with grating monochromator (wavelength of 377 nm) and an irradiation distance of 1 mm. During the photocatalytic POM reaction, the light beam from the light source was directly irradiated onto the catalyst bed. At the same time, heating was produced with a furnace tube to provide sufficient heat until the catalyst was ignited. The reaction products were analyzed by a GC-TCD equipped with columns, Porapak Q ($H_{2,}$ O_2, and CO) and Molecular Sieve 5A (CO_2, H_2O, and CH_3OH). The methanol conversion (C_{MeOH}), hydrogen selectivity (S_{H2}), and CO selectivity (S_{CO}) obtained from different reaction conditions are defined as follows:

$$C_{MeOH} = (n_{MeOH,in} - n_{MeOH,out})/n_{MeOH,in} \times 100\%$$

$$S_{H2} = n_{H2}/(n_{H2O} + n_{H2}) \times 100\%$$

$$S_{CO} = n_{CO}/(n_{CO} + n_{CO2}) \times 100\%$$

3. Results and discussion

3.1. Characterization of catalysts

The physicochemical characteristics of A_xCZ (x% Au loadings (x = 0 − 10), 30% Cu, (100-x-30)% Zn) catalysts are shown in Table 1. From the ICP-MS result, the actual metal loading was expected and there was a less than 10% loss of Au.

Comparing XRD patterns of ZnO NPs as shown in Fig. 1(a)–(g), only hexagonal wurtzite ZnO peaks and no excess impurities peaks were observed. The size of ZnO NPs, derived by estimating a ZnO (101) peak at 36.1^0 through the Debye-Scherer formula, displayed 8.32, 6.51, 8.08, 10.08, 9.33, 10.7, and 10.08 nm respectively, for $A_{10}CZ$, A_4CZ, A_3CZ A_2CZ, CZ, and ZnO (as listed in Table 1). Fig. 1 (a)–(d) demonstrates that a gold diffraction peak of (1 1) at 38.2^0 overlapped with a copper oxide diffraction peak at 38.8^0 on catalyst with gold. A gold (2 0) diffraction peak at 44.4^0 was not found, which should be highly dispersed and small in size.

The element distribution of A_xCZ was measured by XPS. The abundance of Cu^{2+} (BE of $Cu_{2p3/2}$ = 933–934 eV) and Zn^{2+} (BE of $Zn_{2p3/2}$ = 1021.5-1022.5 eV) was observed on the surface of fresh catalysts. The binding energies of $Au_{4f7/2}$ for Au^0 and Au^{3+} were 83.0-84.12 eV and 85.5–88 eV, respectively [47]. The distribution of Cu on catalyst surfaces, except $A_{10}CZ$, increased with the addition of Au. Moreover, the dispersion of the CuO and surface area improved from

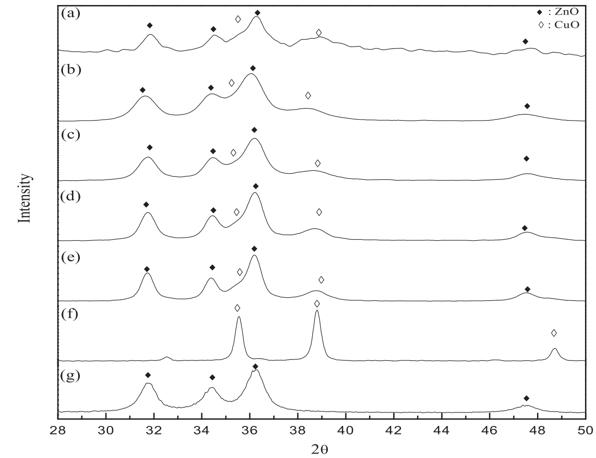

Fig. 1. XRD pattern of: (a) $A_{10}CZ$; (b) A_4CZ; (c) A_3CZ; (d) A_2CZ (e) CZ; (f) CuO; (g) ZnO catalysts.

ca. 26.26% to 33.79%. and 32.86–49.42 m^2/g, respectively. The size of CuO NPs on Au_4CZ was 4.14 nm, which was the smallest compared with other catalysts.

The high-resolution transmission electron microscopy (HR-TEM) images are shown in Fig. 2. The solid black points are Au nanoparticles. The HR-TEM micrograph of CZ (Fig. 2 (a)) clearly shows that the lattice fringes of 0.25 nm correspond to the wurtzite ZnO planes (101). In addition, the size of gold particle over the A_xCZ (Fig. 2(b)–(f)) was well-controlled within ca. 2–5 nm. Generally, 3–10 nm-sized particles, which hold more interface and surface area, are reported to exhibit higher activity [48]. The lattice fringes of 0.23 nm also correspond to the lattice spacing of Au (111) which exhibited high activity for oxidation reactions [49,50].

Fig. 3(d) shows the reduction pattern of CZ. The main peak forward to 205 °C and ending at about 215 °C is associated with reduction of CuO species interacting with the supporter. Fig. 3(a)–(c) shows that the reduction peaks shift to the lower temperature of about 190 °C, which indicates a better reducibility for catalyst with gold [44].

In summary, gold increases Cu dispersion, surface area, and enhances the reducibility of the catalyst, which may further affect the chemisorption and dissociation property of the catalyst.

3.2. Photocatalytic reforming of methanol over gold-promoted, copper-zinc catalyst for low ignition temperature

Fig. 4 shows the performance of catalysts in POM reaction. The C_{MeOH}% increased suddenly at ignition temperature (T_i). The balance temperature (T_b) is defined as the temperature at which the reaction is kept at auto-thermal equilibrium. C_{MeOH} (Fig. 4(a)) and S_{H2} (Fig. 4(b)) of catalysts display in order of $A_4CZ > CZ$ at lower temperature (130–225 °C) without illumination. The T_i could be lowered significantly from 175 °C to 130 °C on gold-promoted CuZn catalyst, but high temperature conditions were still required to achieve good reactivity (ca. ∼99% of C_{MeOH}, ∼90% of S_{H2} at 250 °C for A_4CZ).

The performance of catalysts during photocatalytic POM (photo-POM) reaction (illuminated for 200 min and temperature maintained at ignition temperature) is shown in Fig. 4. Obviously, T_i can be further lowered via illumination from 130 °C to 70 °C and 175 °C to 150 °C on A_4CZ and CZ catalysts, respectively. In addition, A_4CZ catalyst of C_{MeOH} reached 70% at 70 °C (T_i) and the performance was better than CZ catalyst; e.g., C_{MeOH} from 82% to 92% and S_{H2} from 80% to 91%, respectively, at 150 °C.

3.3. The relationship of ignition temperature and gold promoter

To represent the effect of gold on photocatalytic activity and

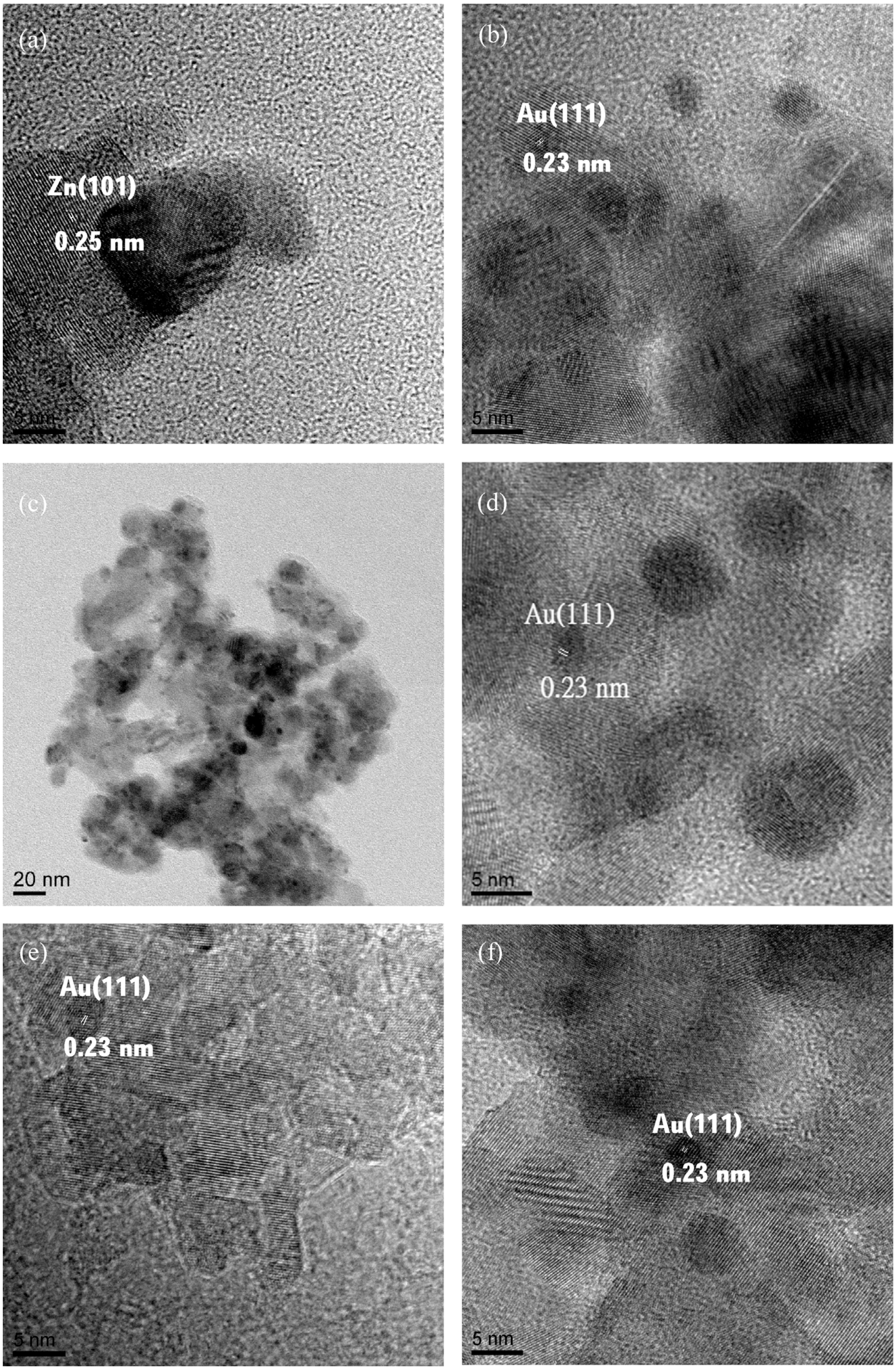

Fig. 2. TEM image of: (a) CZ; (b) $A_{10}CZ$; (c) A_4CZ; (d) A_4CZ; (e) A_3CZ; (f) A_2CZ.

ignition temperature, the time-on-stream of A_xCZ catalysts with various gold contents (2–10 wt.%) in photo-POM reaction is shown in Fig. 5. During the photo-POM reaction, light and heat were continuously provided to keep the outside and ignition temperatures the same. We found that the ignition temperature decreased to 90 °C and 70 °C with the increasing of gold content up to 2% and 4%, respectively, in the photo-POM reaction. Even at room temperature (35 °C), the ignition phenomenon could be observed if the content of gold was increased to more than 10% ($A_{10}CZ$). Moreover, if heat was maintained at ignition temperature (35, 70, 90 °C), the reaction temperature could reach equilibrium at the 120, 170, and 193 °C for $A_{10}CZ$, A_4CZ, and A_2CZ catalysts, respectively.

In Fig. 5(a), the A_2CZ exhibited the lowest value of C_{MeOH}. The C_{MeOH} of $A_{10}CZ$ was less than A_4CZ at the lowest T_b (only at 120 °C) during photo-POM reaction. High temperature can accelerate the decomposition of methanol. Fig. 5(b) shows S_{H2} proportional to the amount of gold, which could be up to 95% for $A_{10}CZ$ catalyst. In another important finding related to carbon monoxide selectivity (S_{CO}), Fig. 5(c) shows that S_{CO} decreased with increasing gold content, except for A_2CZ.

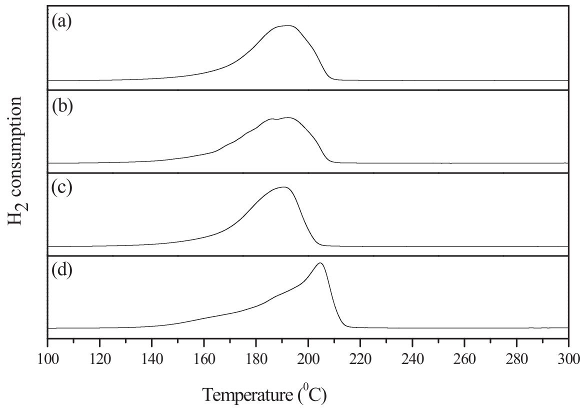

Fig. 3. H_2 temperature programmed reduction of: (a) A_4CZ; (b) A_3CZ; (c) A_2CZ (d) CZ catalyst.

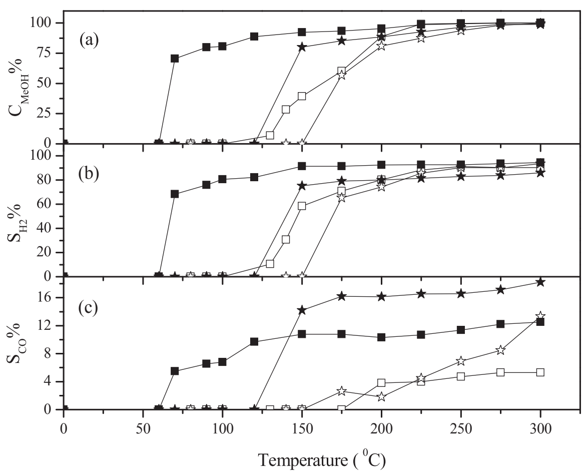

Fig. 4. The temperature profile of the: (a) Methanol conversion (C_{MeOH}); (b) Hydrogen selectivity (S_{H2}); and (c) Carbon monoxide selectivity (S_{CO}) of catalysts in POM reaction w/wo illuminating. (□) A_4CZ, (☆) CZ catalyst without illuminating. (■) A_4CZ, (★) CZ with illuminating.

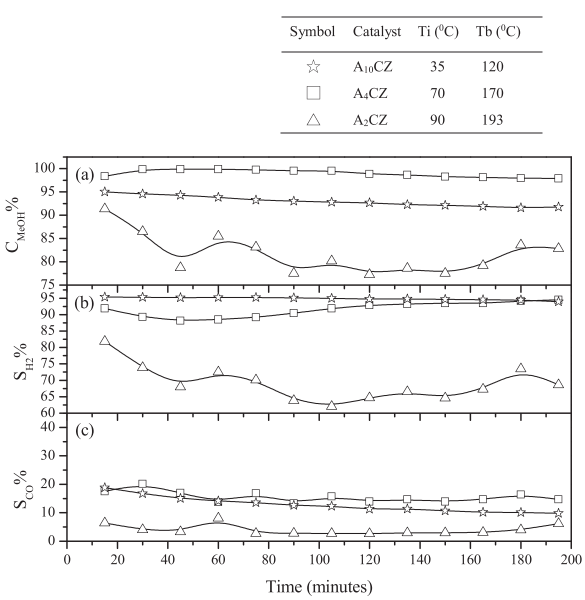

Fig. 5. Time-on-stream of the photo-POM reaction was irradiated for 200 min and heat was continuously provided to keep the outside temperature the same as the ignition temperature over different gold contents. (☆)$A_{10}CZ$, (□)A_4CZ, (△)A_2CZ catalysts: (a) Methanol conversion; (b) Hydrogen selectivity; (c) Carbon monoxide selectivity.

Table 2
The percentage of copper and gold species of CZ, A_4CZ catalyst by in-situ XANES data fitting.

Sample	Cu Species (%)			Au Species (%)	
	Cu^{2+}	Cu^{+}	Cu^0	Au^{3+}	Au^0
CZ-fresh	100	0	0	–	–
CZ- 3 h[a]	20	42.2	37.8	–	–
CZ- photo–10 min[b]	2.3	39.3	60.7	–	–
CZ- photo–3 h	3.6	39.4	57.1	–	–
A_4CZ-fresh	100	0	0	52.9	47.1
A_4CZ- 3 h[c]	17.1	44.6	38.3	32.6	67.4
A_4CZ- photo–10 min[d]	10.4	42.7	49.2	14.6	85.4
A_4CZ- photo–3 h	7.3	38.1	55.2	14	86

[a] The POM reaction over CZ catalyst during 3 h at ignition temperature (170 °C).
[b] The photo-POM reaction over CZ catalyst during 10 min at ignition temperature (150 °C).
[c] The POM reaction over A_4CZ catalyst during 3 h at ignition temperature (130 °C).
[d] The photo-POM reaction over A_4CZ catalyst during 10 min at ignition temperature (70 °C).

3.4. Mechanism study of Au/CuO/ZnO catalyst during photocatalytic POM reaction

Many studies indicate that the electric charge state might influence catalytic performance; e.g., Cu^{2+} is inactive [51–54] and results in catalytic deactivation during the POM reaction. However, photo-POM might induce electron migration and change the distribution of electrically charged copper and gold. Therefore, variation in the electrical charge of copper and gold species on the CZ and A_4CZ catalysts during photo-POM was measured by in-situ X-ray absorption spectroscopy (XAS). The percentages of copper and gold species of CZ and A_4CZ catalysts measured by in-situ XANES (shown in SI, Fig. S1) data fitting are summarized in Table 2. We observed 100% of Cu^{2+}, which was regarded as non-active state toward reforming [51], in the fresh catalysts. In the initial illumination for 10 min at T_i (150 °C), 60.7% Cu^0 and 39.3% Cu^+ were found on CZ catalyst (CZ-photo–10 min). Generally, Cu^+- Cu^0 are active sites [54]. The copper species varied within the reduction-oxidation mechanism $Cu^{2+} \rightarrow Cu^+ + Cu^0$ according to XANES data. However, a slight decrement of Cu^0 and an increment of Cu^{2+} were observed on the CZ-photo–3 h sample after 3 h of photo-POM reaction, which suggests catalytic deactivation over time [44,51–53,55]. Interestingly, CZ-photo–3 h catalyst, via a three-hour illumination, exhibited more Cu^0 (57.1%) than CZ-3h(POM reaction without illumination, 37.8% of Cu^0). This suggests that the electrons might be accelerated, thus transferring to the copper via illumination; which makes the copper species into an electric-charge storage that releases electrons to gold quickly. Thus, the whole reaction for photo-POM could be enhanced at lower temperature.

For A_4CZ catalyst, the fitted XANES spectra (Table 2) shows that the most plentiful copper species was Cu^{2+} in the fresh A_4CZ catalyst. Only 38.3% of Cu^0 and 44.6% Cu^+ were observed during the POM reaction (without illumination) for 3 h at 130 °C on the A_4CZ–3 h sample. However, in the initial 10 min of illumination, copper species were reduced to 49.2% Cu^0, 42.7% Cu^+ on A_4CZ-photo–10 min, and then Cu^0 species increased to 55.2% after 3 h (sample A_4CZ-photo–3 h). From this observation, we hypothesized that the gold promoter, a photo-sensitive material with high electrical capacity [56], can act as an electron acceptor to promote the Cu electron transfer, which results in less Cu^0 on A_4CZ-photo sample than on CZ-photo sample. To prove the electronic transition mechanism, the UV–vis absorption spectra of ZnO, CZ and A_4CZ were recorded and are shown in Fig. 6. The excitonic absorption band of CZ and A_4CZ was red-shifted to ca. 377 and 400 nm, respectively, and the intensity of broad absorption edge from 450 to 1000 nm was $A_4CZ > CZ$. Observation verified that copper and gold on ZnO surface were responsible for the absorption in the visible region,

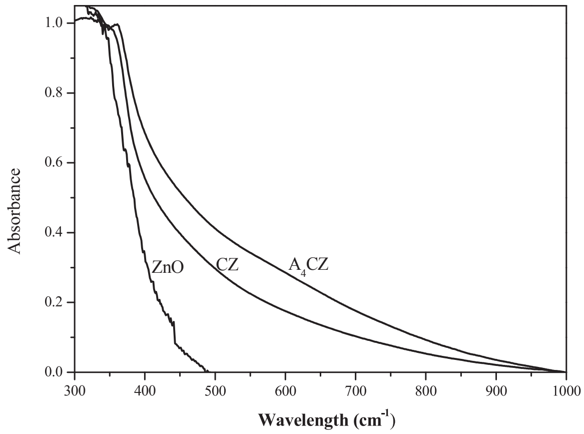

Fig. 6. The UV–vis absorption spectra of ZnO, CZ and A_4CZ samples.

which might enhance the photocatalytic reaction at low temperature.

Fig. S2 shows the Au L_3-edge XANES spectra. The white-line intensity of $HAuCl_4$ is positioned around 11923 eV, which is attributed to the 2p − 5d transition [57]. The Au L_3-edge XANES fitting result is shown in Table 2. The fresh A_4CZ sample composition is 52.9% Au^{3+} and 47.1% Au^0. The XPS measurement also shows similar results. From the Au_{4f} deconvolution in Figure S-3 and Table 1, all catalysts exhibit peaks assigned as Au^0 and Au^{3+}. Interestingly, the ratio of Au^0/Au^{3+} increases as the Au loading amount increases. A lower portion of Au^{3+} ions might induce higher catalytic activity due to lesser amount of the inactive Au^{3+} ionic gold species [58]. During POM reaction, the white-line intensity in the Au L_3-edge XANES spectra was decreased, indicating that Au^{3+} ion was reduced to Au^0. The cationic gold was found to be less stable and reduced to metallic gold under the reaction conditions. After 3 h of POM reaction, Au species was reduced to 67.4% of Au^0 on the A_4CZ–3 h sample. In addition, we found that more Au species were reduced to Au^0 in the photo-POM reaction; e.g., 85.4% Au after 10 min. Because gold has a high electrical capacity and its Fermi level (5.53 eV) is lower than copper (7.00 eV), electrons might go through the copper and transfer to Au during photo-POM reaction when excited from a ZnO valance band to a conduction band.

To further realize the mechanisms of the surface species or intermediates on the Au/Cu/Zn catalysts during the photo-POM reaction, the in-situ diffuse reflectance infrared Fourier transform spectroscopy (DRIFTS) spectra were investigated. The spectra (Fig. 7) of the surface species on the A_4CZ catalyst were detected during POM reaction w/or w/o illuminating at 150 °C for 30 min. Fig. 7(a) shows that after exposing CH_3OH/O_2 gas without UV, methoxy groups ($-OCH_3$), with bands at 2930, 2850, 1400 and 1060 cm^{-1}, were assigned [59], and isolated hydroxyl groups, with peaks at 3500–3800 cm^{-1} [60], were observed. After 30 min of POM reaction, carbonate ($-CO_3$) with peaks of 1600–1900, 1100–1300 cm^{-1}, and water at 3300 cm^{-1} were observed. More energy for desorption was needed and the reaction resulted in less S_{H2}% [61–65].

However, when the temperature was raised to 150 °C under illumination, $-OCH_3$ received photo-holes to form $-OCH_2$ radicals (Eq. (1)) [66]. Fig. 7 (d)–(e) shows that within 4–5 min, adsorption bands in the region of 3000–3500, 2800–2900 and 1260–1500 cm^{-1} were in an intermediate state of $-OCH_2$ incorporated with oxygen to generate $-OCH_2O$, which produced hydrogen bonding with $-OH$ group appearing at 3200–3500 cm^{-1} (Eq. (2)). The intermediate compound, $-OCH_2O$, converted rapidly to formate and was observed in less than 10 min. Hence, the methoxy group fluxes were found to decrease quickly. According to G. Jacobs et al. [67], absorption bands in the region of 1250–1450 cm^{-1} are the OCO stretching mode. In Fig. 7 (e)–(f), during photo-POM reaction of 15–30 min, formate groups (–OCOH) appeared around 1250–1450, 1600–1750, and 2800–2999 cm^{-1}. Some bands around 1600–1750 ascribed to C=O species. This clearly proved that the intermediate formate groups (–OCOH) could be found at low temperatures during photo-POM reaction. With time increased to 30 min, the reaction reached equilibrium, and the methoxy group was consumed completely as the

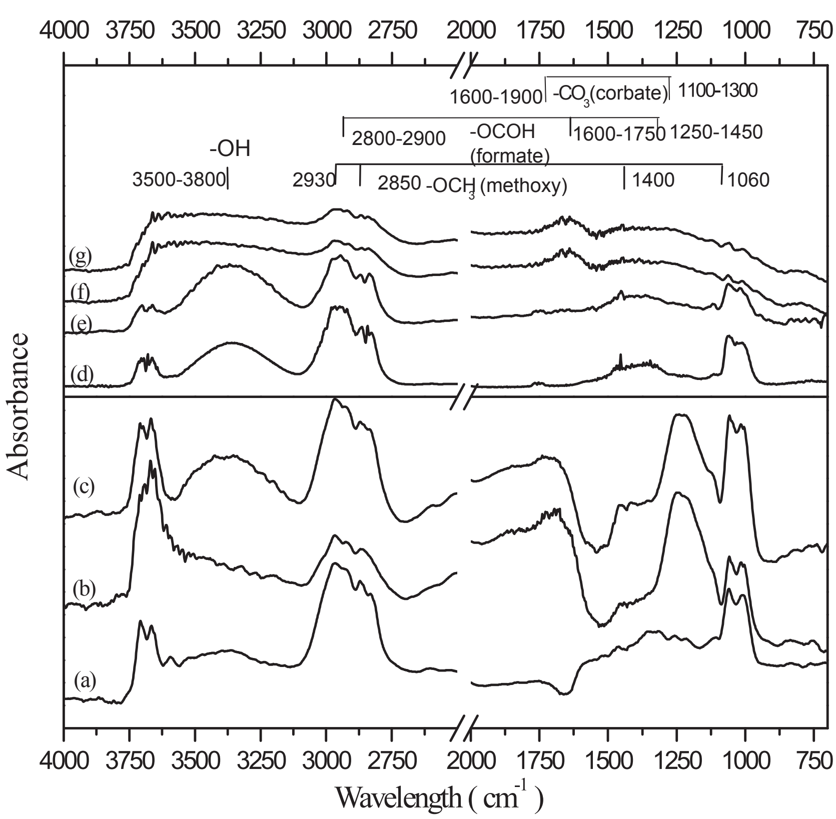

Fig. 7. In-situ DRIFT spectra of surface species evolution during POM reaction w/wo illumination on A_4CZ catalyst at 150 °C for 30 min: (a) before reaction; (b) POM 5 min; (c) POM 30 min; (d) photo-POM 4 min; (e) photo-POM 5 min; (f) photo-POM 15 min; (g) photo-POM 30 min.

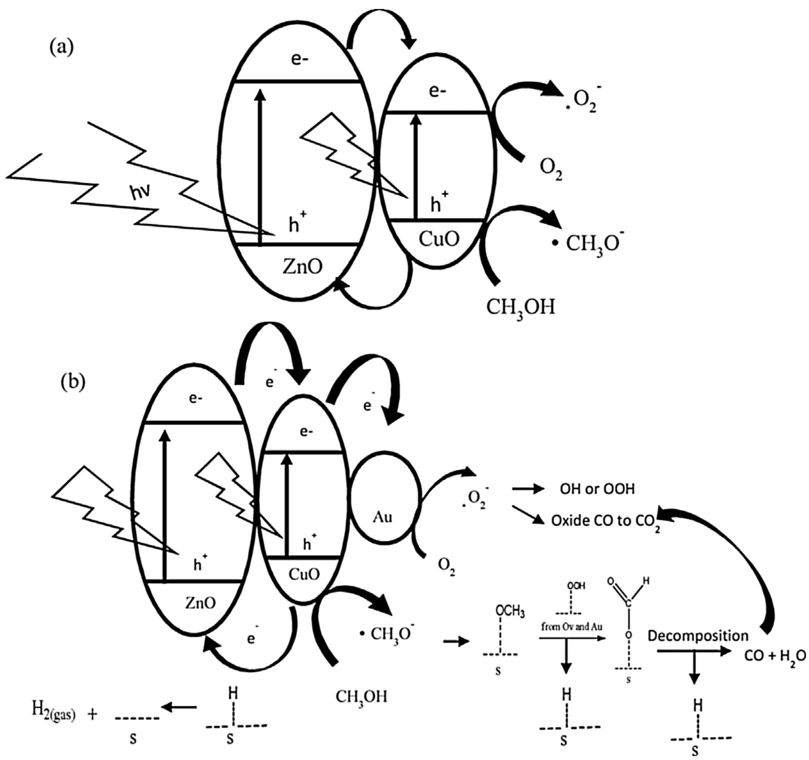

Scheme 1. The mechanism for photo-POM over CZ and A_4CZ catalyst.

1060 cm^{-1} peak disappeared (Eq. (3)). The total adsorbed formate species decomposed violently to H_2 and CO (Eq. (4)).

Integration of XAS and IR results are summarized in Scheme 1. First, ZnO was irradiated by UV light, and electrons (e^-) in the valence band were excited to the conduction band, leaving corresponding holes (h^+) in the VB. Electrons were easily trapped by copper then transferred to gold, thus storing and releasing electrons to process the reduction-oxidation mechanism $Cu^{2+} \rightarrow Cu^+ + Cu^0$. It was observed that more methoxy species formed on the surface of the catalyst. At the same time, a higher ratio of Au^0 species also promoted the reducibility of catalyst. These −OH and −O* resulted in the adsorbed $-OCH_3$ oxidizing to –OCOH (formate), then decomposing quickly to H_2 and CO over A_4CZ catalyst [37]. Moreover, gold-promoted catalyst could be not only photogenerated charge carriers, but also could increase the absorption intensity of light energy; thereby a performance better than CZ catalyst was shown in photo-POM reaction at a lower ignition temperature (70 °C).

4. Conclusions

A_xCZ catalysts in photo-POM reaction were effectively triggered at low temperature (e.g., T_i for A_4CZ is 70 °C) and performed (C_{MeOH} 92%, S_{H2} 91% for A_4CZ) better than CZ catalyst at 150 °C. Gold promoter could lower the T_i, and $A_{10}CZ$ could ignite at room temperature (35 °C) and show 95% C_{MeOH} and 95% S_{H2} at 120 °C. The effect of illumination over 19.3% Cu^0 was observed on CZ catalyst during POM reaction via 3 h of illumination. Moreover, more than 18.6% of Au species were reduced to Au^0 in POM reaction via 3 h of illumination. This suggests that illuminated conditions speed up electron transfer to copper. The high electrical capacity of cationic gold was found to act as an electron acceptor to promote the Cu electron transfer, causing copper species charge storage and quick release to gold. Active Cu^0 and Cu^+ were produced under photo-POM, forming unstable intermediate (–OCOH) and rapidly decomposing to hydrogen on A_4CZ. Thus, photo-triggered catalytic reforming of methanol over gold-promoted, copper-zinc catalyst could enhance the entire reaction at lower temperature (70 °C).

Acknowledgement

The authors acknowledge funding from the Ministry of Science and Technology (MOST), Taiwan (105-3113-E-007-002-).

References

[1] Z.F. Wang, J.Y. Xi, W.P. Wang, G.X. Lu, Selective production of hydrogen by partial oxidation of methanol over Cu/Cr catalysts, J. Mol. Catal. A Chem. 191 (2003) 123–134.
[2] M.L. Cubeiro, J.L.G. Fierro, Selective production of hydrogen by partial oxidation of methanol over ZnO-supported palladium catalysts, J. Catal. 179 (1998) 150–162.
[3] L.Y. Mo, X.M. Zheng, C.T. Yeh, Selective production of hydrogen from partial oxidation of methanol over silver catalysts at low temperatures, Chem. Commun. (2004) 1426–1427.
[4] T.J. Huang, S.W. Wang, Hydrogen-production via partial oxidation of methanol over copper-zinc catalysts, Appl. Catal. 24 (1986) 287–297.
[5] D.W. Jing, J.W. Shi, P. Meyrueis, H. Zhou, Semiconductor-based photocatalytic, photoelectrochemical, and photovoltaic solar-energy conversion, Sci. World J. 2014 (2014) 1. Article ID 695204.
[6] M. Schubnell, I. Kamber, P. Beaud, Photochemistry at high temperatures — Potential of ZnO as a high temperature photocatalyst, Appl. Phys. A Mater. 64 (1997) 109–113.
[7] C. Zhao, S.H. Zhong, Preparation and characterization of Cu/ZnO-TiO_2 coupled-semiconductor photocatalyst, Chin. J. Inorg. Chem. 20 (2004) 1131–1136.
[8] D.W. Jing, R. Li, M.C. Liu, L.J. Guo, Copper-doped ZnO/ZnS core/shell nanotube as a novel photocatalyst system for photocatalytic hydrogen production under visible light, Int. J. Nanotechnol. 8 (2011) 446–457.
[9] A.M. Hussein, L. Mahoney, R. Peng, H. Kibombo, C.M. Wu, R.T. Koodali, R. Shende, Mesoporous coupled ZnO/TiO_2 photocatalyst nanocomposites for hydrogen generation, J. Renew. Sustain. Energy 5 (2013).
[10] A. Tiwari, I. Mondal, U. Pal, Visible light induced hydrogen production over thiophenothiazine-based dye sensitized TiO_2 photocatalyst in neutral water, RSC Adv. 5 (2015) 31415–31421.
[11] F.S. Liu, R. Ji, M. Wu, Y.M. Sun, Hydrogen production from water splitting using perylene dye-sensitized Pt/TiO_2 photocatalyst, Acta Phys. Chim. Sin. 23 (2007) 1899–1904.
[12] Y.J. Yuan, F. Wang, B. Hu, H.W. Lu, Z.T. Yu, Z.G. Zou, Significant enhancement in photocatalytic hydrogen evolution from water using a MoS_2 nanosheet-coated ZnO heterostructure photocatalyst, Dalton T. 44 (2015) 10997–11003.
[13] C.M. Janet, S. Navaladian, B. Viswanathan, T.K. Varadarajan, R.P. Viswanath, Heterogeneous wet chemical synthesis of superlattice-Type hierarchical ZnO architectures for concurrent H_2 production and N_2 reduction, J. Phys. Chem. C 114 (2010) 2622–2632.
[14] C. Karunakaran, V. Rajeswari, P. Gomathisankar, Photodeposited surface Ag on ZnO nanocrystals and the optical, electrical, photocatalytic, and bactericidal

properties, Synth. React. Inorg. M. 41 (2011) 369–375.

[15] T.Y. Peng, H.J. Lv, P. Zeng, X.H. Zhang, Preparation of ZnO nanoparticles and photocatalytic H_2 production activity from different sacrificial reagent solutions, Chin. J. Chem. Phys. 24 (2011) 464–470.

[16] M.S. Oh, J. Cho, W.K. Choi, ZnO-based photoconductive UV detector, Elec. Soc. S 2002 (2002) 112–116.

[17] Y.Y. Lv, L.S. Yu, H.Y. Huang, H.L. Liu, Y.F. Feng, Preparation, characterization of P-doped TiO_2 nanoparticles and their excellent photocatalytic properties under the solar light irradiation, . Alloy Compd. 488 (2009) 314–319.

[18] A. Kudo, Y. Miseki, Heterogeneous photocatalyst materials for water splitting, Chem. Soc. Rev. 38 (2009) 253–278.

[19] K. Yamato, A. Iwase, A. Kudo, Photocatalysis using a wide range of the visible light spectrum: hydrogen evolution from doped $AgGaS_2$, ChemSusChem 8 (2015) 2902–2906.

[20] W.Q. Cui, C.H. Xu, S.D. Zhang, L.R. Feng, S.J. Lu, F.L. Qiu, Hydrogen evolution by photocatalysis of methanol vapor over Ti-beta, J. Photoch. Photobio. A 175 (2005) 89–93.

[21] N.L. Wu, M.S. Lee, Enhanced TiO_2 photocatalysis by Cu in hydrogen production from aqueous methanol solution, Int. J. Hydrogen Energy 29 (2004) 1601–1605.

[22] K. Domen, S. Naito, T. Onishi, K. Tamaru, Photocatalytic decomposition of liquid water on a nio srtio3 catalyst, Chem. Phys. Lett. 92 (1982) 433–434.

[23] M. Hirata, K. Shimamoto, E. Sakai, N. Koike, K. Mizuochi, E. Watanabe, H. Mizuno, K. Nakamura, M. Hara, M. Kawana, Polymyositis, dermatomyositis and systemic sclerosis patients have relative left ventricular hypertrophy, J. Card. Fail. 11 (2005) S307.

[24] Z.L. Liu, J.C. Deng, J.J. Deng, F.F. Li, Fabrication and photocatalysis of CuO/ZnO nano-composites via a new method, Mater. Sci. Eng. B Adv. 150 (2008) 99–104.

[25] B.X. Li, Y.F. Wang, Facile synthesis and photocatalytic activity of ZnO-CuO nanocomposite, Superlattice Microst. 47 (2010) 615–623.

[26] Y. Sakata, T. Yamamoto, T. Okazaki, H. Imamura, S. Tsuchiya, Generation of visible light response on the photocatalyst of a copper ion containing TiO_2, Chem. Lett. (1998) 1253–1254.

[27] P. Gomathisankar, K. Hachisuka, H. Katsumata, T. Suzuki, K. Funasaka, S. Kaneco, Enhanced photocatalytic hydrogen production from aqueous methanol solution using ZnO with simultaneous photodeposition of Cu, Int. J. Hydrogen Energy 38 (2013) 11840–11846.

[28] J. Bandara, C.P.K. Udawatta, C.S.K. Rajapakse, Highly stable CuO incorporated TiO_2 catalyst for photocatalytic hydrogen production from H_2O, Photoch. Photobio. Sci. 4 (2005) 857–861.

[29] Z.B. Hai, N. El Kolli, J.F. Chen, H. Remita, Radiolytic synthesis of Au-Cu bimetallic nanoparticles supported on TiO_2: application in photocatalysis, New J. Chem. 38 (2014) 5279–5286.

[30] M. Hakamada, M. Yuasa, T. Yoshida, F. Hirashima, M. Mabuchi, Visible-light photocatalysis of ZnO deposited on nanoporous Au, Appl. Phys. A Mater. 114 (2014) 1061–1066.

[31] R. Kaur, B. Pal, Size and shape dependent attachments of Au nanostructures to TiO_2 for optimum reactivity of Au-TiO_2 photocatalysis, J. Mol. Catal. A Chem. 355 (2012) 39–43.

[32] A.A. Madhavan, G.G. Kumar, S. Kalluri, J. Joseph, S. Nagarajan, S. Nair, K.R.V. Subramanian, A. Balakrishnan, Effect of embedded plasmonic Au nanoparticles on photocatalysis of electrospun TiO_2 nanofibers, J. Nanosci. Nanotechnol. 12 (2012) 7963–7967.

[33] J. Lu, H.H. Wang, D.L. Peng, T. Chen, S.J. Dong, Y. Chang, Synthesis and properties of Au/ZnO nanorods as a plasmonic photocatalyst, Physica E 78 (2016) 41–48.

[34] X.Y. Zhan, Y.J. Bao, F.M. Wang, Q.S. Wang, Z.Z. Cheng, Z.X. Wang, K. Xu, Z.Y. Fang, J. He, Surface plasmon resonance enhanced light absorption of Au decorated composition-tuned $ZnO/Zn_xCd_{1-x}Se_yTe_{1-y}$ core/shell nanowires for efficient H_2 production, Appl. Phys. Lett. 106 (2015).

[35] S.Y. Du, Z.Y. Li, Enhanced light absorption of TiO_2 in the near-ultraviolet band by Au nanoparticles, Opt. Lett. 35 (2010) 3402–3404.

[36] S. Sarina, E.R. Waclawik, H. Zhu, Photocatalysis on supported gold and silver nanoparticles under ultraviolet and visible light irradiation, Green Chem. 15 (2013) 1814.

[37] J. Greaves, L. Al-Mazroai, A. Nuhu, P. Davies, M. Bowker, Photocatalytic methanol reforming on Au/TiO_2 for hydrogen production, Gold Bull. 39 (2006) 216–219.

[38] S. Dulnee, A. Luengnaruemitchai, R. Wanchanthuek, Activity of Au/ZnO catalysts prepared by photo-deposition for the preferential CO oxidation in a H_2-rich gas, Int. J. Hydrogen Energy 39 (2014) 6443–6453.

[39] V. Subramanian, E.E. Wolf, P.V. Kamat, Green emission to probe photoinduced charging events in ZnO-Au nanoparticles. Charge distribution and fermi-level equilibration, J. Phys. Chem. B 107 (2003) 7479–7485.

[40] N. Udawatte, M. Lee, J. Kim, D. Lee, Well-Defined Au/ZnO nanoparticle composites exhibiting enhanced photocatalytic activities, ACS Appl. Mater. Inter. 3 (2011) 4531–4538.

[41] P. Li, Z. Wei, T. Wu, Q. Peng, Y.D. Li, Au-ZnO hybrid nanopyramids and their photocatalytic properties, J. Am. Chem. Soc. 133 (2011) 5660–5663.

[42] X.Y. Liu, M.H. Liu, Y.C. Luo, C.Y. Mou, S.D. Lin, H.K. Cheng, J.M. Chen, J.F. Lee, T.S. Lin, Strong metal-Support interactions between gold nanoparticles and ZnO nanorods in CO oxidation, J. Am. Chem. Soc. 134 (2012) 10251–10258.

[43] Y.J. Huang, K.L. Ng, H.Y. Huang, The OSRM reaction over gold promoted copper zinc catalyst, J. Chin. Inst. Eng. 34 (2011) 11–17.

[44] Y.J. Huang, K.L. Ng, H.Y. Huang, The effect of gold on the copper-zinc oxides catalyst during the partial oxidation of methanol reaction, Int. J. Hydrogen Energy 36 (2011) 15203–15211.

[45] S. Brunauer, P.H. Emmett, E. Teller, Adsorption of gases in multimolecular layers, J. Am. Chem. Soc. 60 (1938) 309–319.

[46] A. Gervasini, S. Bennici, Dispersion and surface states of copper catalysts by temperature-programmed-reduction of oxidized surfaces (s-TPR), Appl. Catal. A Gen. 281 (2005) 199–205.

[47] P. Kaminski, M. Ziolek, Mobility of gold, copper and cerium species in Au Cu/Ce, Zr-oxides and its impact on total oxidation of methanol, Appl. Catal. B Environ. 187 (2016) 328–341.

[48] V. Petkov, Y. Ren, S.Y. Shan, J. Luo, C.J. Zhong, A distinct atomic structure-catalytic activity relationship in 3–10 nm supported Au particles, Nanoscale 6 (2014) 532–538.

[49] Z. Huo, C.-k. Tsung, W. Huang, X. Zhang, P. Yang, Sub-two nanometer single crystal Au nanowires, Nano Lett. 8 (2008) 2041–2044.

[50] B.K. Min, A.R. Alemozafar, M.M. Biener, J. Biener, C.M. Friend, Reaction of Au (111) with sulfur and oxygen: scanning tunneling microscopic study, Top. Catal. 36 (2005) 77–90.

[51] L. Alejo, R. Lago, M.A. Pena, J.L.G. Fierro, Partial oxidation of methanol to produce hydrogen over Cu-Zn-based catalysts, Appl. Catal. A Gen. 162 (1997) 281–297.

[52] Y.C. Lin, L.T. Fan, S. Shafie, K.L. Hohn, B. Bertok, F. Friedler, Catalytic pathways identification for partial oxidation of methanol on copper-zinc catalysts: $CH_3OH + 1/2O_2$<-> $CO_2 + 2H_2$, Ind. Eng. Chem. Res. 47 (2008) 2523–2527.

[53] J. Agrell, H. Birgersson, M. Boutonnet, I. Melian-Cabrera, R.M. Navarro, J.L.G. Fierro, Production of hydrogen from methanol over Cu/ZnO catalysts promoted by ZrO_2 and Al_2O_3, J. Catal. 219 (2003) 389–403.

[54] L.S. Kau, K.O. Hodgson, E.I. Solomon, X-ray absorption-edge and exafs study of the copper sites in zno methanol synthesis catalysts, J. Am. Chem. Soc. 111 (1989) 7103–7109.

[55] J. Agrell, M. Boutonnet, J.L.G. Fierro, Production of hydrogen from methanol over binary Cu/ZnO catalysts – part II. Catalytic activity and reaction pathways, Appl. Catal. A Gen. 253 (2003) 213–223.

[56] S.S. Rayalu, D. Jose, M.V. Joshi, P.A. Mangrulkar, K. Shrestha, K. Klabunde, Photocatalytic water splitting on Au/TiO_2 nanocomposites synthesized through various routes: enhancement in photocatalytic activity due to SPR effect, Appl. Catal. B Environ. 142 (2013) 684–693.

[57] I. Berrodier, F. Farges, M. Benedetti, M. Winterer, G.E. Brown, M. Deveughele, Adsorption mechanisms of trivalent gold on iron- and aluminum-(oxy)hydroxides. Part 1: X-ray absorption and Raman scattering spectroscopic studies of Au(III) adsorbed on ferrihydrite, goethite, and boehmite, Geochim. Cosmochim. Acta 68 (2004) 3019–3042.

[58] A. Simakov, I. Tuzovskaya, A. Pestryakov, N. Bogdanchikova, V. Gurin, M. Avalos, M.H. Farías, On the nature of active gold species in zeolites in CO oxidation, Appl. Catal. A Gen. 331 (2007) 121–128.

[59] D. Bianchi, T. Chafik, M. Khalfallah, S.J. Teichner, Intermediate species on zirconia supported methanol aerogel catalysts. 2. Adsorption of carbon-monoxide on pure zirconia and on zirconia containing zinc-oxide, Appl. Catal. A Gen. 105 (1993) 223–249.

[60] C. Cao, K.L. Hohn, Study of reaction intermediates of methanol decomposition and catalytic partial oxidation on Pt/Al_2O_3, Appl. Catal. A Gen. 354 (2009) 26–32.

[61] C.D. Cao, K.L. Hohn, Study of reaction intermediates of methanol decomposition and catalytic partial oxidation on Pt/Al_2O_3, Appl. Catal. A Gen. 354 (2009) 26–32.

[62] K. Kahler, M.C. Holz, M. Rohe, J. Strunk, M. Muhler, Probing the reactivity of ZnO and Au/ZnO nanoparticles by methanol adsorption: a TPD and DRIFTS study, ChemPhysChem 11 (2010) 2521–2529.

[63] Q. Sun, C.W. Liu, W. Pan, Q.M. Zhu, J.F. Deng, In situ IR studies on the mechanism of methanol synthesis over an ultrafine Cu/ZnO/Al_2O_3 catalyst, Appl. Catal. A Gen. 171 (1998) 301–308.

[64] S.T. Yong, K. Hidajat, S. Kawi, The roles of Cu, Zn and Mn in $Cu_{0.5}Zn_{0.5}Mn_2O_4$ spinel-lattice catalyst for methanol decomposition, Catal. Today 131 (2008) 188–196.

[65] D. Bianchi, T. Chafik, M. Khalfallah, S.J. Teichner, Intermediate species on zirconia supported methanol aerogel catalysts. 5. Adsorption of methanol, Appl. Catal. A Gen. 123 (1995) 89–110.

[66] C.C. Chuang, C.C. Chen, J.L. Lin, Photochemistry of methanol and methoxy groups adsorbed on powdered TiO_2, J. Phys. Chem. B 103 (1999) 2439–2444.

[67] G. Jacobs, B.H. Davis, In situ DRIFTS investigation of the steam reforming of methanol over Pt/ceria, Appl. Catal. A Gen. 285 (2005) 43–49.